Contactless, photoinitiated snap-through in azobenzene-functionalized polymers

M. Ravi Shankar[a,1], Matthew L. Smith[b], Vincent P. Tondiglia[c], Kyung Min Lee[c], Michael E. McConney[c], David H. Wang[c], Loon-Seng Tan[c], and Timothy J. White[c,1]

[a]Department of Industrial Engineering, University of Pittsburgh, Pittsburgh, PA 15261; [b]Department of Engineering, Hope College, Holland, MI 49423; and [c]Air Force Research Laboratory, Materials and Manufacturing Directorate, Wright Patterson Air Force Base, OH 45433

Edited by Timothy M. Swager, Massachusetts Institute of Technology, Cambridge, MA, and approved October 8, 2013 (received for review July 12, 2013)

Photomechanical effects in polymeric materials and composites transduce light into mechanical work. The ability to control the intensity, polarization, placement, and duration of light irradiation is a distinctive and potentially useful tool to tailor the location, magnitude, and directionality of photogenerated mechanical work. Unfortunately, the work generated from photoresponsive materials is often slow and yields very small power densities, which diminish their potential use in applications. Here, we investigate photoinitiated snap-through in bistable arches formed from samples composed of azobenzene-functionalized polymers (both amorphous polyimides and liquid crystal polymer networks) and report orders-of-magnitude enhancement in actuation rates (approaching 10^2 mm/s) and powers (as much as 1 kW/m^3). The contactless, ultra-fast actuation is observed at irradiation intensities <<100 mW/cm^2. Due to the bistability and symmetry of the snap-through, reversible and bidirectional actuation is demonstrated. A model is developed to elucidate the underlying mechanics of the snap-through, specifically focusing on isolating the role of sample geometry, mechanical properties of the materials, and photomechanical strain. Using light to trigger contactless, ultrafast actuation in an otherwise passive structure is a potentially versatile tool to use in mechanical design at the micro-, meso-, and millimeter scales as actuators, as well as switches that can be triggered from large standoff distances, impulse generators for microvehicles, microfluidic valves and mixers in laboratory-on-chip devices, and adaptive optical elements.

photochemistry | elastic instability

Transduction of light into work in photoresponsive polymeric materials does not require contact and can be remotely triggered potentially over long distances. The ease with which light can be manipulated spatio-temporally in intensity, phase, and polarization further distinguish this novel input stimulus in mechanically active systems. Prior demonstrations of photomechanical effects in polymeric materials have used both photothermal (1) and photochemical (2–4) mechanisms. Photochemical routes, in nearly all cases using the photoisomerization of azobenzene, are particularly interesting because they offer broader opportunities for modulating photomechanical responses with irradiation wavelength and polarization.

The basis of light-to-work transduction (actuation) in azobenzene-functionalized polymeric materials is the rate and efficiency of the isomerization/reorientation of the embedded azobenzene chromophores. The extent of azobenzene isomerization (efficiency) is considerably lessened by embedding this photochromic moiety in a polymeric material—evident in the work of Morawetz, which contrasts the kinetics and photostationary state concentration of azobenzene photoisomerization in dilute solution, plasticized, and bulk forms (5). Photoisomerization in polymeric materials becomes less efficient and slower with increase in storage modulus (6). Accordingly, photomechanical power densities of monolithic polymeric actuators are limited unless circumvented as demonstrated in this study. Prior work that has sought to increase the magnitude of photomechanical work output via quasi-static, photochemically induced deflections of azobenzene-functionalized polymers (with moduli ranging from 0.6 to 2 GPa) are stymied by the timescales of actuation (typically tens of seconds to a few hours) (7). Tailoring the polymer network structure, crosslink densities, and connectivity of azobenzene units within the network have proven to affect the photomechanical actuation (7, 8), with a few reports using high irradiation intensities (>200 mW/cm^2) to yield combined photothermal and photochemical effects to accelerate the actuation (9).* Photothermal mechanisms inevitably soften the materials, which can be deleterious to potential application of photomechanical effects in an integrated system (e.g., load-bearing).

In addition to informing the underlying mechanics of instructive examples from the natural world, such as the closing of the Venus fly-trap (10) or Hummingbird's beak (11), understanding and exploiting the mechanics of snap-through (also referred to as snap-buckling) can be useful for engineering active structures (12–16). Our demonstration of ultrafast actuation via photomechanical instabilities may offer a unique design paradigm, where an otherwise passive unit is prompted into motion by a directed photonic source. Here, the photoactuation is hard-coded via mechanical design, and its progression occurs without any onboard control-loops or power sources. Application niches requiring spatially

Significance

Photomechanical effects in polymers are distinguished by the ease with which actinic light can be regulated to contactlessly trigger the magnitude and directionality of mechanical adaptivity with spatio-temporal control. The materials examined to date have not demonstrated power densities or actuation speeds necessary for applications seeking to exploit the promise of wirelessly triggered actuation. Using mechanical design, we employ two classes of azobenzene-functionalized polymers and demonstrate contactless snap-through of bistable arches realizing orders-of-magnitude enhancement in the actuation rates (~10^2 mm/s) and powers (~1 kW/m^3) under moderate irradiation intensities (<<100 mW/cm^2). The experimental characterization of the snap-through is supported with modeling that elucidates the effect of geometry, mechanical properties, and photogenerated strain on the actuation rate and energy output.

Author contributions: M.R.S., M.L.S., and T.J.W. designed research; M.R.S., M.L.S., V.P.T., K.M.L., and M.E.M. performed research; K.M.L., D.H.W., and L.-S.T. contributed new reagents/analytic tools; M.R.S. and M.L.S. analyzed data; and M.R.S., M.L.S., and T.J.W. wrote the paper.

The authors declare no conflict of interest.

This article is a PNAS Direct Submission.

[1]To whom correspondence may be addressed. E-mail: ravishm@pitt.edu or timothy.white.24@us.af.mil.

This article contains supporting information online at www.pnas.org/lookup/suppl/doi:10.1073/pnas.1313195110/-/DCSupplemental.

*In contrast, the approach described here is generic in allowing for a step change in the actuation rates and power densities by exploiting photomechanical elastic instabilities (snap-buckle/snap- through) that are wirelessly triggered under nearly isothermal irradiation in samples composed from a range of azobenzene-functionalized polymers, including high-modulus azobenzene-functionalized polyimides that are otherwise characterized by extremely slow (hours) photomechanical responses.

resolved, contactless actuation that are especially defined by discrete states may be impacted in implementations such as surfaces with switchable topographies, active micromirror/microlens arrays (13), and optically driven microsystems where bistable electromechanical structures are otherwise being considered; for example, in integrated optical systems for fiber switches (17) or even modular elements defined by discrete geometric states to constitute future light-driven binary robotic systems (18).

Experiment

To demonstrate actuation by photomechanical snap-through, we use both glassy azobenzene-functionalized polyimides (Fig. 1*A*) and glassy azobenzene-functionalized liquid crystal polymer networks (LCNs; Fig. 1*B*) to confirm the responses observed here are generalizable to multiple classes of photoresponsive systems. Exposure to linearly polarized light of suitable wavelength is known to generate strains in the vicinity of the irradiated surface in these materials and the resulting gradient of the strains through the thickness manifests macroscopic deformation, which has often been examined by observing the bending of irradiated cantilevers as illustrated in Fig. 1 (7). Here, strip-like samples (typically ~20 mm × 1 mm × 15 μm) of these materials were clamped at the ends, initially L_o apart and then compressed slightly to a distance L until they buckled to create bistable arches similar to that illustrated in the inset in Fig. 2. This structure is characterized by two stable, but symmetric positions: either arched upward or downward. Earlier studies have revealed the existence of geometric parameters that bias such mechanical systems toward snap-through when deformed, both in the context of engineering design (19) and in analysis of analogous mechanisms in the natural world (10). Thus, using the geometry illustrated in Fig. 2 enables this work to be contrasted to prior examinations of snap-through in naturally occurring systems, as well as enables tractability of modeling this first demonstration of phototriggered instability. In this geometry, the transitions between the bistable states involves an inversion of the strain field where an otherwise tensile strain at a surface becomes compressive when the arch flips inside-out under the action of an external impetus. This switch-over can occur either gradually via a smooth transition or over a significantly smaller timescale via elastic instabilities. When arches are approximated as arcs of a circle fitted to their center, a predisposition toward snap-through instability is encapsulated by a dimensionless geometric parameter $\alpha = \theta^2 R/2h$, where θ is the angle of the sector formed by the circle fit to the arch, R is the radius of curvature, and $2h$ is the thickness of the arch (Fig. 2). This parameter is analogous to those considered elsewhere (10, 19), where it has been demonstrated that large $\alpha >> 1$ increases the predisposition for snap-through between the two symmetrical stable positions. In this study, effective α values typically >100 are considered. The optical setup in Fig. 2, using a 445-nm light source (a commercially available handheld laser pointer), allows for illuminating these samples at their center with a circular light beam of diameter (d) from either the top or the bottom with polarization that is parallel to the long axis of the arch by flipping a mirror. An upwardly arched sample was illuminated from above, whereas a downwardly arched sample (Fig. 3) would be illuminated from below.

Results and Discussion

Photomechanical responses were examined in arches created from the azobenzene-functionalized polyimides and azobenzene-functionalized LCNs of the monodomain and twisted nematic orientations. Fig. 3 illustrates the response of a film composed of an azobenzene-functionalized polyimide similar to those characterized in references (20, 21) displaced into a bistable arch with $\alpha \sim 130$. The sample is illuminated from the bottom with 445-nm irradiation at an intensity of 18 mW/cm^2 and a diameter (d) of 5 mm, the center of which was aligned to the midpoint of the arch. Irradiation with 445-nm light induces contraction at the exposed surface, via the *trans–cis–trans* reorientation mechanism associated with these irradiation conditions (blue-green light, linear polarization parallel to $\mathbf{e}_1$) (7). Negligible photothermal effects are anticipated at this intensity (7).

Due to the large absorption coefficient of the materials, light is absorbed nonuniformly through the thickness. In this work, sample thicknesses were selected such that actinic light is extinguished within the depth of the samples. Accordingly, the photogenerated strain gradient that forms through the sample thickness (mirroring the intensity gradient) modifies the curvature of the arch. In this case, a transformation of the geometry of the sample occurs over 8.4 s until a "critical configuration" is reached (Fig. 3*C*). This geometry is a precursor to snap-through, which immediately ensues on continuous irradiation wherein the arch turns inside-out to reach the upwardly

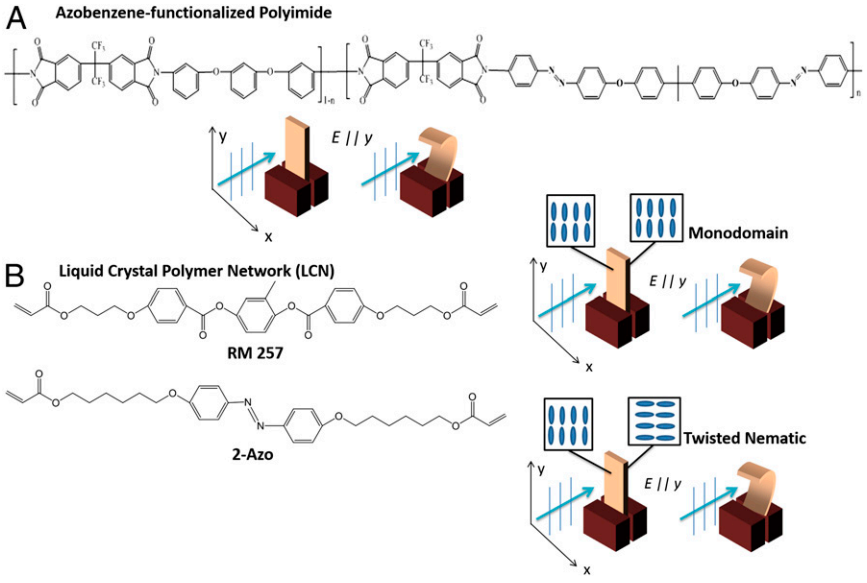

Fig. 1. Azobenzene-functionalized polymers examined in this study. (*A*) Molecular structure of an azobenzene-functionalized polyimide that develops surface contractile strains when exposed to 445-nm light. The principal strains are developed parallel to the polarization direction of the light. (*B*) Monodomain and twisted nematic liquid crystal polymers that are copolymerized with azobenzene-functionalized cross-linkers. Contractile strains are induced when the direction of the polarization is parallel to the orientation of the mesogens.

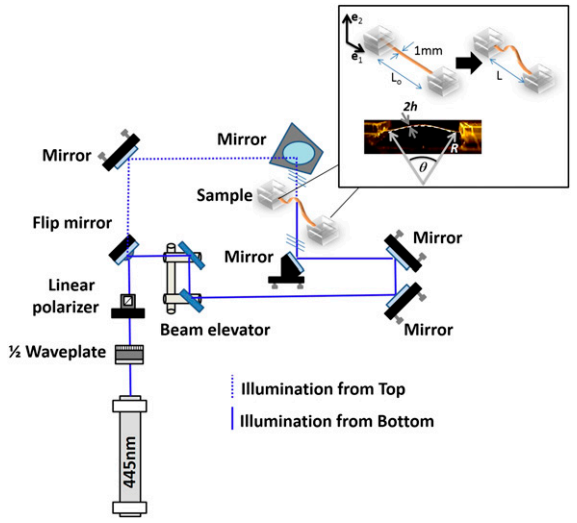

Fig. 2. Experimental setup used for irradiating arches created from photoactive materials from the top and bottom using a 445-nm laser with polarization set parallel to the long-axis of the arch ($\mathbf{e}_1$). (*Inset*) Creation of a bistable arch that is examined for photomechanical snap-through in this study.

convex, stable configuration illustrated in Fig. 3 *D* and *F* (Movie S1).[†]

At each point along the sample, the curvature κ_c from Fig. 3*C* and κ_a from Fig. 3*A* were calculated via curve fitting to the deformed samples to estimate the variation of strains at the irradiated surface, $(\kappa_c - \kappa_a)h$, along the $\mathbf{e}_1$ axis. Fig. 3*B* shows the change in the strain state at each point of the surface, as a result of the gradual accumulation of strains following illumination, between the states in Fig. 3 *C* and *A*. Just before snap-through, contractile strains are induced over the shaded region of the sample in Fig. 3*B*. Outside this contractile region, the tensile strains are found to increase beyond that in the prior configuration to create the asymmetric geometry in Fig. 3*C* that is at the edge of instability (critical configuration). Subsequently, continuous irradiation triggers rapid transformation via snap-through into the upwardly arched configuration. Fig. 3*E* illustrates the change in the strain value on the illuminated surface of the arch between the snapped-through configuration in Fig. 3*F* and that just before the instability. The bending strain energy (U) corresponding to each of the geometries (Fig. 3 *A–F*) can be estimated from the empirical measurement of the local curvature $\kappa(x_i)$ at discrete points (x_i) of the beam. The bending strain energy is given by $U = \sum_i -\frac{EI}{2}\kappa^2(x_i)\Delta x_i$, where E is the elastic modulus, I is the second moment of area of the cross section, and the interval between the discrete points of measurement is $\Delta x_i = x_{i+1} - x_i$. The energy difference between the states in Fig. 3 *C* and *A* was measured to be 22 nJ, which is attributable to the photogenerated strain energy as the arch was deformed to the edge of instability. This measurement relies on the profile of the arch and therefore measures only the contributions from bending assuming Eulerian beam theory. The energy released during snap-through was computed by measuring the difference between the strain energies in Fig. 3 *C* and *F* as 5.7 nJ that is generated over a stroke length of ∼1.7 mm at the center of the sample. For the geometry of the film that was used in this study, this corresponds to a specific energy release of ∼26 J/m^3. Although this method does not account for photoinduced changes in natural length of the material, it nonetheless provides a reasonable estimate of specific energy release and, as will be discussed later, is in agreement with model predictions.

The ultrafast mechanics of the snap-through was examined by imaging with a high-speed camera. Fig. 4 illustrates the evolution of the arch in 3.4-ms intervals as it proceeds through the snap-through from the edge of instability (critical configuration, at t_{cr}). Ultrafast actuation occurs in ∼10 ms in the azobenzene-functionalized polyimide samples within one integral jump (Movie S2). The snap-through in this experiment is characterized by a stroke length of ∼1 mm with a velocity (measured near the center of the sample) reaching ∼100 mm/s. High-speed imaging clarifies the "double image" apparent in Fig. 3*D* (at 30 fps) as simply motion blur and not oscillation. Using the high-speed measurements, the geometry in Fig. 3 is estimated to undergo snap-through in 17 ms, and the specific power delivered as kinetic energy during the photomechanical snap-through is ∼1.5 kW/m^3. Prior examination of related azobenzene-functionalized polyimide materials in cantilever or tensile geometries is typified by slow responses (hours) and small strain values (0.1% or less).

We also examined the generalizability of this approach to azobenzene-functionalized LCNs, whose photomechanical response can be modulated by the relative orientation of the nematic director with the polarization of the actinic light (7, 22). Alignment of the anisotropy of these materials to the geometry of the sample can allow for tailored responses. The behavior of monodomain and twisted nematic LCNs was examined by creating arches, analogous to that in Figs. 2 and 3. Snap-through was observed when the nematic director of the LCN was parallel to the long axis of the sample and irradiated with linearly polarized 445-nm light polarized parallel to the nematic director. On irradiation, the arch underwent a distortion (Fig. 5 *A* and *B*) that was quite reminiscent of that encountered in the polyimides, and after reaching the critical configuration at the edge of instability, ultrafast actuation ensued (Fig. 5*D*). The capability of repeated, bidirectional snap-through is illustrated in Fig. 5 *E–H*. Subsequent to the upward snap-through observed in Fig. 5 *A–D*,

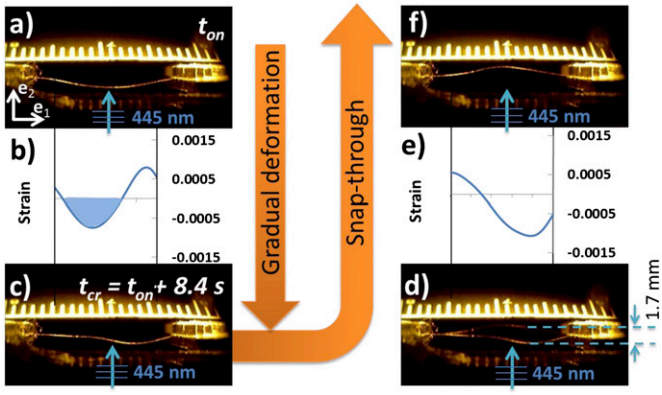

Fig. 3. Progression of photomechanical snap-through in the arch-shaped azobenzene-polyimide samples as revealed by imaging from the side (along $\mathbf{e}_1 \times \mathbf{e}_2$). (*A*) Original arch that is illuminated from the bottom with the polarization set parallel to $\mathbf{e}_1$. (*B*) Change in the bending strains at the irradiated surface before and after 8.4 s of irradiation that is calculated from measurement of curvatures at each point along the arch. (*C*) Geometry at the snap-through threshold, after 8.4 s of irradiation. (*D*) Onset of ultrafast snap-through from the threshold, where the double-image is an artifact due to motion-blur. (*E*) Change in the bending strains at the irradiated surface before and after snap-through and (*F*) final geometry after the snap-through. A scale with millimeter graduations is shown next to the sample (Movie S1).

[†]In addition to the quasi-static approach to instability via continuous irradiation examined here, it is possible to accumulate the photogenerated strains in articulated irradiation steps, where the superposition of photogenerated strains from each step advances the sample closer to instability. As a corollary, suitably designed prior irradiation can be envisaged for priming samples for snap-through and then, when needed, a shorter irradiation can trigger the ultrafast actuation of the primed geometry.

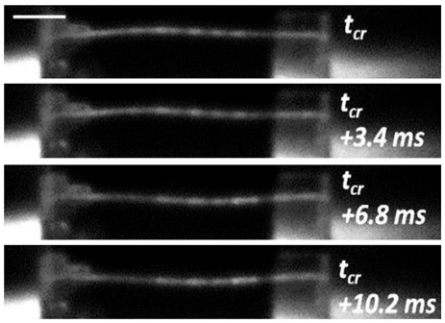

Fig. 4. High-speed imaging that shows the completion of the snap-through in ~10 ms (Movie S2). (Scale bar, 3 mm.)

the sample was illuminated from the top (Fig. 2) to return the sample to the original down state via snap-through apparent in Fig. 5 *E*–*H*. From our experimental examination of a range of photoresponsive materials, the high modulus polyimide (4 GPa) proportionately enhances both the energy released from snap-through and the time for snap-through (which scales in proportion to $\sim\sqrt{\rho/E}$, where ρ is the density) (10). However, the ability to manipulate the local spatial anisotropy to design domain and defect structures that can be designed to optimize the material for specific elastic instabilities are intriguing future avenues only available to the LCN materials (23–26).

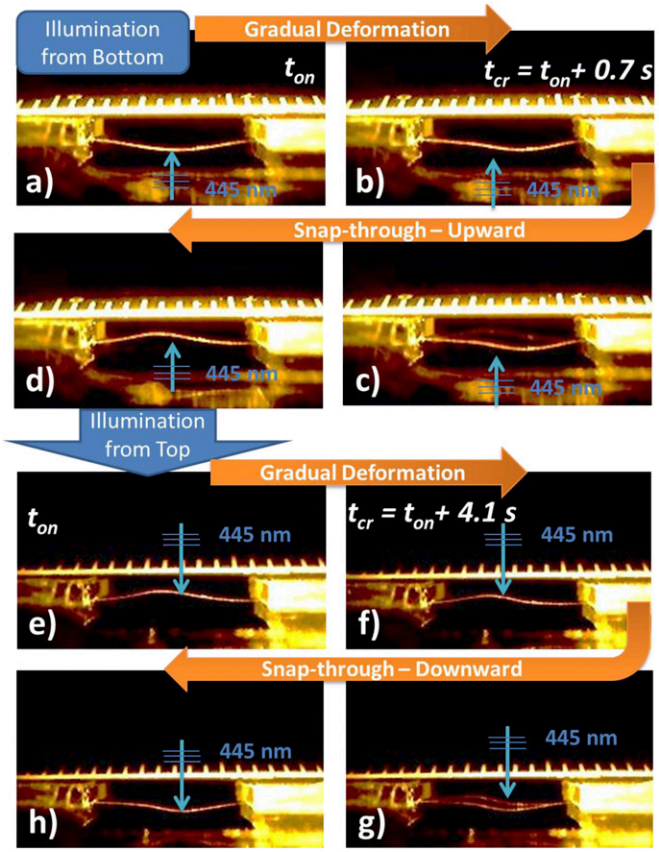

Fig. 5. Bidirectional snap-through in monodomain LCN sample. (*A*) Original geometry is illuminated from the bottom. (*B*) Geometry at the snap-through threshold that is reached via gradual deformation following irradiation. (*C*) Onset of snap-through upward to reach (*D*) the final geometry. (*E*) After snap-through, illumination is switched on from the top. (*F*) Gradual change in geometry occurs to reach the threshold. (*G*) This is followed by onset of downward snap-through, and (*H*) the final geometry is reached after the to-and-fro snap-through (Movie S3).

To facilitate the interpretation of our experimental results, we use a geometrically exact, planar rod model (27) of the photoinitiated snap-through. Here, we examine the quasi-static mechanics as a function of the geometry and material response leading up to the edge of the elastic instability. In the orthonormal coordinate system (Fig. 2), $\{\boldsymbol{e}_1, \boldsymbol{e}_2\}$, the centerline of the beam is given by $\{X_1\boldsymbol{e}_1 : X_1 \in [0, L]\}$ and the location of material points through the thickness are given by $\{X_2\boldsymbol{e}_2 : X_2 \in [-h, h]\}$ (see Fig. S1). The governing equations for this type of beam are

$$n_1' - n_2\kappa = 0, \quad [1]$$

$$n_2' + n_1\kappa = 0, \quad [2]$$

$$m' + \nu_1 n_2 = 0, \quad [3]$$

where, n_1 and n_2 are the internal forces normal and parallel to the cross section, respectively, m is the internal moment, $\nu_1 - 1$ gives the axial strain, and κ is the curvature of the beam. Solutions for the arches with the desired geometry were computed numerically, and then a strain field due to stimulus from light was applied (*SI Text*). The photomechanical contractile strain was assumed to take the form $\epsilon_{ph} = \beta I_o(X_1)\exp(-DX_2)$, where $I_o(X_1)$ is the incident intensity of light, D is the inverse of the attenuation length of the light, X_2 is the variable distance through the thickness, and β, termed the photocompliance, is the proportionality constant relating intensity of light to strain (28, 29). For this work, $I_o(X_1)$ is a boxcar function centered near the middle of the strip and with a width of 5 mm corresponding to the beam diameter of the laser and outside this region of irradiation, $\epsilon_{ph} = 0$. The constitutive relations in this model obey the relations

$$n_1 = \int_{-h}^{h} \sigma_{11} dX_2, \quad [4]$$

$$m = \int_{-h}^{h} X_2\sigma_{11} dX_2, \quad [5]$$

where $\sigma_{11} = \epsilon E$, and the total strain field is given by

$$\epsilon = \kappa X_2 + (\nu_1 - 1) - I_o(X_1)\beta e^{-DX_2}. \quad [6]$$

The simulations (Fig. 6) predict an evolution of the geometry that coincides with that observed in experiment (Fig. 3). For a list of parameter values used in the simulations, see Table S1. The changes in the bending strains that were measured in Fig. 3 from the geometry of the beam were also found to coincide with the model. The strain energy differences that were calculated from the model are also found to be in agreement with the empirical measurements, including that for the energy release during snap-through that is calculated from the difference in the internal stored energy between the configuration at the edge of instability and the final snapped-through state.

The model was also used to calculate the magnitude of the photogenerated strains that are required at the irradiated surface to induce the snap-through. The empirical analysis of the profile of the samples measures bending strains that are manifested due to the inducement of the surface photogenerated strains and their gradients (which are difficult to measure directly and are hence inferred from the model). Simulations were performed for a range of arch geometries and the photogenerated strain at

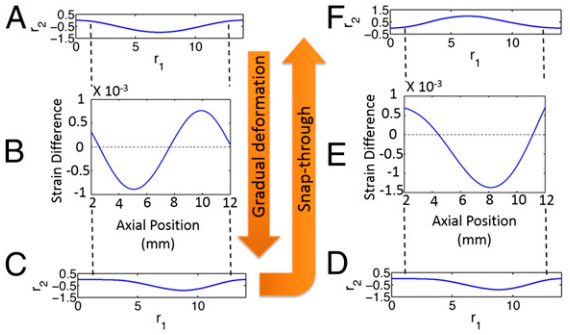

Fig. 6. Computed configurations of an azobenzene-functionalized polyimide arch. (*A*) The original buckled arch with no irradiation. (*B*) The calculated strain difference between *A* and *C* at the surface accumulated during irradiation to reach the snap-through threshold. (*C*) The configuration at the edge of instability as revealed by the simulation. (*D*) The configuration at the threshold that was then used to compute the snapped-through configuration separately. (*E*) Strain difference before and after the snap-through. (*F*) Final snapped-through geometry. Configurations (*A*, *C*, *D*, and *F*) were calculated using the numerical simulations where photoinduced changes to the natural curvature are accounted for. Strain differences (*B* and *E*) were computed from curve fits to the configuration to compare with the empirically measured strain differences. Note the coincidence of this simulation with the empirical observations in Fig. 3. All spatial units are in millimeters.

the irradiated surface (e_{ph}) required for reaching the edge of instability for the azobenzene-polyimide and azo-LCN (Fig. 7*A*). These results are nondimensionalized for a range of L/L_o and d/L_o values, where d is the diameter of the irradiating light beam. The model predicts an increasing photogenerated strain for inducing the instability as L/L_o values become smaller. This dependence is expected because reducing L/L_o would produce increasingly steep arches that require a greater perturbation from the stable state to induce the snap-through. The prediction of increased threshold with increasing d/L_o is attributable to the asymmetric perturbation via bending during irradiation would decline as an increasing fraction of the beam is irradiated. Note that the photogenerated strain required for inducing snap-through in the higher-modulus polyimide (~4 GPa) is greater than that for the lower-modulus LCN (~1 GPa).

It is also apparent that the value of the required photogenerated strain decreased with increasing L/L_o, expectedly converging to zero as L/L_o approaches 1. During this convergence, we also note the decreasing sensitivity of e_{ph} to the geometry and sample material when L/L_o increases. The implications of this insensitivity became apparent when experiments were performed with samples of LCN and polyimide samples with $L/L_o = 0.99$ and $d/L_o = 0.35$ values. When we tracked the time (t_{cr}) for the onset of instability following the start of irradiation, we found it to vary in inverse proportion to the intensity of the irradiation (Fig. 7*B*). Fig. 7*A* offers a rationalization for this observation, where we find that photogenerated strain required for triggering snap-through is quite comparable for the various samples and in the range of ~0.0015–0.002 for the geometries considered here. If we assume that for the irradiation conditions used here the accumulation of the surface strains occurs at approximately the same rate, where e_{ph}/t_{cr} is on the same order as ζI_o, then the variation of t_{cr} in inverse proportion of I_o is expected. For the variation observed here, we estimate ζ to be $\sim 2 \times 10^{-5}$ cm^2/mJ. The model was also used to calculate the variation of the specific energy that is released via photoinitiated snap-through to guide the design of actuator systems. Fig. 7*C* shows the energy released as a function of L/L_o and d/L_o for LCN and polyimide systems. The variation of the energy release follows the trend observed with the threshold strain for snap-through, including the convergence of the various conditions as L/L_o approaches 1. The decrease in the specific energy release with increasing L/L_o across the conditions mirrors the variation in the e_{ph} in Fig. 7*A*. This trend is expected considering that the energy released during snap-through is directly related to that accumulated during the irradiation. Results of simulations in Fig. 7*C* suggest opportunities for magnifying the specific energy release across orders of magnitude by examining a broader range of L/L_o and d/L_o values than those fabricated in this study. A future examination of these conditions might expand design opportunities beyond those envisaged here. Although we demonstrated photoinitiated snap-through in the simpler arches here, it is also possible to envision other geometries and end-support/clamping conditions that can modulate the susceptibility of undergoing snap-through. For example, if geometry similar to that illustrated in Fig. 3*C* or Fig. 6*C* was formed as a starting geometry, the time necessary to reach the critical configuration and trigger snap-through would be eliminated. Such a structure would still be bistable and thus bidirectional. Fabrication protocols for creating such geometries in azobenzene-functionalized polyimide and LCN systems remain to be resolved for realizing these geometries, as well their integration in functional device modules.

Conclusions

This work demonstrates ultrafast, wirelessly triggered actuation in photoresponsive, azobenzene-functionalized polymeric materials

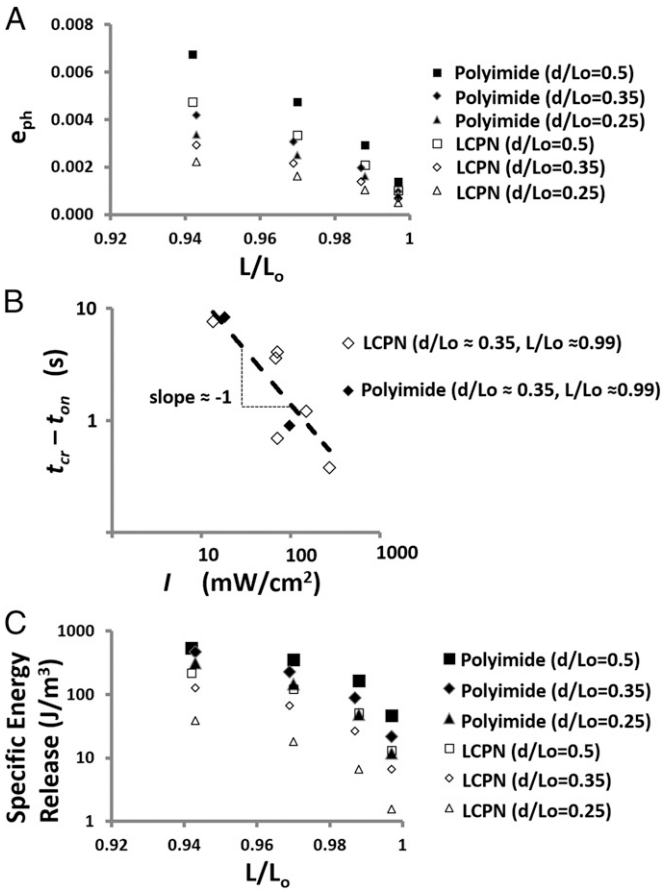

Fig. 7. Using the model to examine the effect of geometry on the threshold for inducing photomechanical snap-through and the resulting energy output. (*A*) Role of L/L_o and d/L_o on the critical photogenerated strain (e_{ph}) required for inducing snap-through in polyimide and LCN samples. (*B*) Empirically measured variation of time for inducing snap-through in LCN and polyimide arches with $L/L_o = 0.99$ and $d/L_o = 0.35$, as a function of the intensity of irradiation. (*C*) Computationally predicted specific energy released from snap-through as a function of geometry for polyimide and LCN.

observed as snap-through in bistable structures. Substantial enhancements in actuation rates and power densities are generated at modest intensities of irradiation in samples composed of azobenzene-functionalized polyimide and azobenzene-functionalized LCNs. In the bistable geometries, irradiation induces surface contractile strains that perturb the structure while increasing the mechanical strain energy. When the structure reaches a stability threshold, ultrafast snap-through ensues and the structure reaches the second stable state. It is also shown that switching the direction of illumination can induce bidirectional snap-through to achieve reversible actuation. The enhancements demonstrated here in the polyimide and the LCN materials are generalizable to other photoresponsive materials, where deployment of suitable mechanical designs can offer step-change enhancements in actuation characteristics. Computational models are used to rationalize these observations and to identify the effect of geometry on the threshold for inducing the snap-through and the achievable energy output. The models, which encapsulated the empirical observations, also point to mechanical designs for achieving orders-of-magnitude higher specific energies and powers than those observed here. The ability to tailor the actuation characteristics in a manner suggested by these models can help use these actuators as unit cells in integrated photoactuated systems—such as planar lattices composed of such bistable structures to create active surfaces, creating morphing structures by stacking 3D lattices of these photoswitchable bistable elements or even as individual binary switches that can be toggled remotely using light. Kinetic energy pulse from the snap-through could offer unique propellant units for novel microvehicles by acting as thrusting legs and might also enable photomechanical triggers for electrical, mechanical, and optical mechanisms. The design principles spawned by this demonstration are likely applicable across length scales, ranging from the milli-, meso-, and micrometer scales, where the ultrafast actuation in bistable, photomechanical units can offer potentially distinctive system opportunities.

Materials and Methods

Synthesis of Azobenzene-Functionalized Polymers. The azobenzene-functionalized polymers examined here were synthesized as previously reported (7, 9, 20). The 1,1,1,3,3,3-hexafluoro-2,2-bis(4-phthalic anhydrido)-propane (6FDA)-based random copolyimide was prepared from 2,2-bis{4-[4-(4-aminophenyl-diazenyl) phenoxy]phenyl}-propane (azobenzene-diamine), 1,3-bis(3-aminophenoxy)benzene (APB), and 6FDA using the same procedures as described previously (20) to generate the imidized polymers. In the material examined here, the stoichiometric ratio of diamines used was 45 mol% azobenzene-diamine and 55 mol% APB. The azobenzene-functionalized liquid crystal polymer networks were prepared by photopolymerization initiated with 1.5 wt% Irgacure 784 with 60 mW/cm^2 of 532-nm irradiation for ∼60 min. The samples examined here were prepared by copolymerizing a formulation composed from 20 wt% of an azobenzene-containing, liquid crystal diacrylate monomer with 78.5 wt% of the liquid crystal diacrylate monomer RM257. The samples were cured in the nematic phase of the prepolymer mixture at 75 °C. The rubbing direction of the self-prepared liquid crystal alignment cells was antiparallel (monodomain) or orthogonal (twisted nematic).

Experimental and Imaging Setup. The optical setup was built using commercially available components sourced (Thorlabs and Newport), and the 445-nm laser source was procured from WickedLasers. Imaging was performed using an Aven Mighty Scope system (at 30 frames/s), and high-speed imaging was performed using a PCO.Edge sCMOS camera. Samples were illuminated using a fiber optic cold light illuminator (Cole-Parmer). Imaging was performed from the side through a glass long-pass filter (Thorlabs) to discern the sample profile during laser irradiation. The laser power was measured using a digital power and energy meter (Thorlabs).

ACKNOWLEDGMENTS. This work was completed at the Air Force Research Laboratory in the Materials and Manufacturing Directorate (AFRL/RX). M.R.S. acknowledges the support of the Air Force Office of Scientific Research (AFOSR) through the American Society for Engineering Education (ASEE) Summer Faculty Fellowship Program in addition to National Science Foundation Grant 1030265. V.P.T., K.M.L., M.E.M., D.H.W., L.-S.T., and T.J.W. acknowledge financial support from AFRL/RX and AFOSR.

1. Ji Y, Huang YY, Rungsawang R, Terentjev EM (2010) Dispersion and alignment of carbon nanotubes in liquid crystalline polymers and elastomers. *Adv Mater* 22(31): 3436–3440.
2. Eisenbach CD (1980) Cis-trans isomerization of aromatic azo chromophores, incorporated in the hard segments of poly(ester urethane)s. *Makromol Chem Rapid Commun* 1(5):287–292.
3. Finkelmann H, Nishikawa E, Pereira GG, Warner M (2001) A new opto-mechanical effect in solids. *Phys Rev Lett* 87(1):015501.
4. Yu Y, Nakano M, Ikeda T (2003) Photomechanics: Directed bending of a polymer film by light. *Nature* 425(6954):145.
5. Paik CS, Morawetz H (1972) Photochemical and thermal isomerization of azoaromatic residues in the side chains and the backbone of polymers in bulk. *Macromol* 5(2): 171–177.
6. Ikeda T, Mamiya J, Yu Y (2007) Photomechanics of liquid-crystalline elastomers and other polymers. *Angew Chem Int Ed Engl* 46(4):506–528.
7. Lee KM, Tabiryan NV, Bunning TJ, White TJ (2012) Photomechanical mechanism and structure-property considerations in the generation of photomechanical work in glassy, azobenzene liquid crystal polymer networks. *J Mater Chem* 22(2):691–698.
8. Kondo M, et al. (2010) Effect of concentration of photoactive chromophores on photomechanical properties of crosslinked azobenzene liquid crystal polymers. *J Mater Chem* 20(1):117–122.
9. Lee KM, et al. (2011) Photodriven, flexural–torsional oscillation of glassy azobenzene liquid crystal polymer networks. *Adv Funct Mater* 21(15):2913–2918.
10. Forterre Y, Skotheim JM, Dumais J, Mahadevan L (2005) How the Venus flytrap snaps. *Nature* 433(7024):421–425.
11. Smith ML, Yanega GM, Ruina A (2011) Elastic instability model of rapid beak closure in hummingbirds. *J Theor Biol* 282(1):41–51.
12. Keplinger C, Li T, Baumgartner R, Suo Z, Bauer S (2012) Harnessing snap-through instability in soft dielectrics to achieve giant voltage-triggered deformation. *Soft Matter* 8(2):285–288.
13. Holmes DP, Crosby AJ (2007) Snapping surfaces. *Adv Mater* 19(21):3589–3593.
14. Giannopoulos G, Monreal J, Vantomme J (2007) Snap-through buckling behavior of piezoelectric bimorph beams: I. Analytical and numerical modeling. *Smart Mater Struct* 16(4):1148–1157.
15. Lee H, Xia C, Fang NX (2010) First jump of microgel: Actuation speed enhancement by elastic instability. *Soft Matter* 6(18):4342–4345.
16. Shahinpoor M (2011) Biomimetic robotic Venus flytrap (*Dionaea muscipula Ellis*) made with ionic polymer metal composites. *Bioinspir Biomim* 6(4):046004.
17. Liu H-B, Chollet F (2009) Moving polymer waveguides and latching actuator for 2 x 2 MEMS optical switch. *J Microelectromech Syst* 18(3):715–724.
18. Hafez M, Lichter MD, Dubowsky S (2003) Optimized binary modular reconfigurable robotic devices. *IEEE/ASME Trans Mechatron* 8(1):18–25.
19. GJelsvik A, Bodner SR (1962) Energy criterion and snap through buckling of arches. *J Eng Mech* 88(5):87–134.
20. Lee KM, et al. (2012) Enhancement of photogenerated mechanical force in azobenzene-functionalized polyimides. *Angew Chem Int Ed Engl* 51(17):4117–4121.
21. Wang DH, et al. (2011) Photomechanical response of glassy azobenzene polyimide networks. *Macromolecules* 44(10):3840–3846.
22. Lee KM, Koerner H, Vaia RA, Bunning TJ, White TJ (2011) Light-activated shape memory of glassy, azobenzene liquid crystalline polymer networks. *Soft Matter* 7(9): 4318–4324.
23. Modes CD, Bhattacharya K, Warner M (2010) Disclination-mediated thermo-optical response in nematic glass sheets. *Phys Rev E Stat Nonlin Soft Matter Phys* 81(6 Pt 1): 060701.
24. Lee KM, Bunning TJ, White TJ (2012) Autonomous, hands-free shape memory in glassy, liquid crystalline polymer networks. *Adv Mater* 24(21):2839–2843.
25. McConney ME, et al. (2013) Topography from topology: Photoinduced surface features generated in liquid crystal polymer networks [published online ahead of print July 21, 2013]. *Adv Mater*, 10.1002/adma.201301891.
26. de Haan LT, Sánchez-Somolinos C, Bastiaansen CMW, Schenning APH, Broer DJ (2012) Engineering of complex order and the macroscopic deformation of liquid crystal polymer networks. *Angew Chem Int Ed Engl* 51(50):12469–12472.
27. Antman SS (2005) *Nonlinear Problems of Elasticity* (Springer, New York), 2nd Ed.
28. Warner M, Mahadevan L (2004) Photoinduced deformations of beams, plates, and films. *Phys Rev Lett* 92(13):134302.
29. van Oosten CL, Harris KD, Bastiaansen CWM, Broer DJ (2007) Glassy photomechanical liquid-crystal network actuators for microscale devices. *Eur Phys J E Soft Matter* 23(3): 329–336.